1 High-temperature series expansion for the single band Hubbard model

In the vicinity of the atomic limit, where the tunneling between sites is small compared to the on-site interactions, the Hubbard model can be treated by considering tunneling as a perturbation. This treatment allows us to gain insight into the different phases that the system can exhibit. This section follows closely after [1, 2].

We work in the grand canonical ensemble, so we include a global chemical potential in the hamiltonian

$$\begin{aligned} H =& \left(U \sum_i n_{i\uparrow} n_{i\downarrow} - \mu \sum_i (n_{i\uparrow} + n_{i\downarrow}) \right) - t \sum_{\langle ij \rangle, \sigma} a^\dagger_{i\sigma} a_{j\sigma} \\ =& H_0 + H_1 \end{aligned} \tag{1}$$

For the unperturbed part, H_0, the grand canonical partition function is

$$Z_0 = \mathrm{Tr} e^{-\beta H_0} \tag{2}$$

Since the unperturbed part is a sum over sites, the partition function becomes a product of the single site partition function: $Z_0 = z_0^k$, for a system with k sites. The single site partition function is easy to evaluate because the trace runs only over the four possible states in a single site $\{|0\rangle, |\uparrow\rangle, |\downarrow\rangle, |\updownarrow\rangle\}$.

$$z_0 = 1 + 2e^{\beta\mu} + e^{\beta(2\mu - U)} = 1 + 2z + z^2 u \tag{3}$$

where we have defined $z = e^{\beta\mu}$ and $u = e^{-\beta U}$. Among the relevant physical quantities that can be obtained are: the number of particles, the number of double occupancies, and the entropy per site. These are obtained from the first derivatives of the grand canonical potential, Ω

$$\Omega = -\frac{\ln Z}{\beta} \tag{4}$$

$$N = -\frac{\partial \Omega}{\partial \mu} \tag{5}$$

$$D = \frac{\partial \Omega}{\partial U} \tag{6}$$

$$S = -\frac{\partial \Omega}{\partial T} \tag{7}$$

Also, from the second derivatives of the grand potential one can obtain the fluctuations in any of these quantities.

For the full hamiltonian, the grand canonical partition function, Z, can be expanded in a perturbation series [1]:

$$\begin{aligned} Z =& \mathrm{Tr} e^{-\beta H} \\ =& Z_0 \left[1 + \sum_{n=1}^{\infty} (-1)^n \int_0^\beta d\tau_1 \int_0^{\tau_1} d\tau_2 \cdots \int_0^{\tau_{n-1}} d\tau_n \langle \tilde{H}_1(\tau_1) \tilde{H}_2(\tau_2) \cdots \tilde{H}_n(\tau_n) \rangle \right] \end{aligned} \tag{8}$$

where the thermal expectation value inside the integral is taken with the unperturbed hamiltonian

$$\langle A \rangle = \mathrm{Tr}(e^{\beta H_0} A)/Z_0 \tag{9}$$

and the tilde means that the operator is evaluated in the interaction picture, for the imaginary time indicated:

$$\tilde{H}_1(\tau) = e^{\tau H_0} H_1 e^{-\tau H_0} \tag{10}$$

Given the series expansion for Z, the grand potential is

$$-\beta\Omega = Z_0 + \sum_{n=1}^{\infty}(-1)^n \int_0^\beta d\tau_1 \int_0^{\tau_1} d\tau_2 \cdots \int_0^{\tau_{n-1}} d\tau_n \langle \tilde{H}_1(\tau_1)\tilde{H}_2(\tau_2)\cdots\tilde{H}_n(\tau_n)\rangle \tag{11}$$

One can see that the n^{th} term in the expansion has n copies of the tunneling part of the hamiltonian. Each application of H_1 in the thermal average results in a particle tunneling to a neighboring site, so we see that there will be a contribution to the expansion only if, after n tunneling events, all the particles come back to their original sites. As a direct consequence, the first order term in the expansion vanishes. The second order in the expansion corresponds to particles tunneling one site over and then coming back. Higher order terms can be represented by diagrams, making it easier to keep track of them. The contribution from orders up to $n = 9$ is shown in [1]. Here we will use up to the second order term to illustrate the phases that appear in the system.

The grand potential to second order is [1, 2]

$$-\beta\Omega_2 = k \ln z_0 + k \left(\frac{\beta t}{z_0}\right)^2 m \left(z + z^3 u + 2z^2 \frac{1-u}{\beta U}\right) \tag{12}$$

where m is the number of nearest neighbors for each lattice site, which in the simple cubic case is $m = 6$. We see that the grand potential is proportional to the number of lattice sites, k, so all the thermodynamic quantities will be expressed per lattice site. The resulting phase diagram is shown in Fig. 1 for a temperature $T/t = 2.5$.

An important path along the phase diagram is the one corresponding to $\mu = U/2$. Along this line, referred to as half-filling, the density is always one particle per site. It can be shown [3] that the phase diagram for the Hubbard model in a bipartite lattice[1] is symmetric when the chemical potential is reflected on the half-filling line. The number of particles per site $n \equiv \langle n_\uparrow + n_\downarrow\rangle$, and the local moment $\langle m^2\rangle \equiv \langle (n_\uparrow - n_\downarrow)^2\rangle$ as a function of chemical potential are given by

$$\begin{aligned} n(U/2 + \delta\mu) &= 2 - n(U/2 - \delta\mu) \\ \langle m^2\rangle(U/2 + \delta\mu) &= \langle m^2\rangle(U/2 - \delta\mu) \end{aligned} \tag{13}$$

The double occupancy, d, does not show the same symmetry in μ, it is given by

$$d \equiv \langle n_\uparrow n_\downarrow\rangle = \frac{n - \langle m^2\rangle}{2} \tag{14}$$

The phase diagram obtained from the high temperature series expansion shows us the three insulating phases that exist in the Fermi-Hubbard model. The vacuum, with zero particles per site is an insulating state, and the Mott insulator and band insulator have exactly one and two particles per site respectively. The fluctuations in particle number vanish for the three insulating states. Also, the chemical potential shows a gap as a function of the density, as shown in Fig. 2. The gap in the chemical potential around $n = 1$ is known as the Mott gap.

[1] A bipartite lattice consists of two sub-lattices A, B such that all neighbors of A are in B and vice-versa. [3]

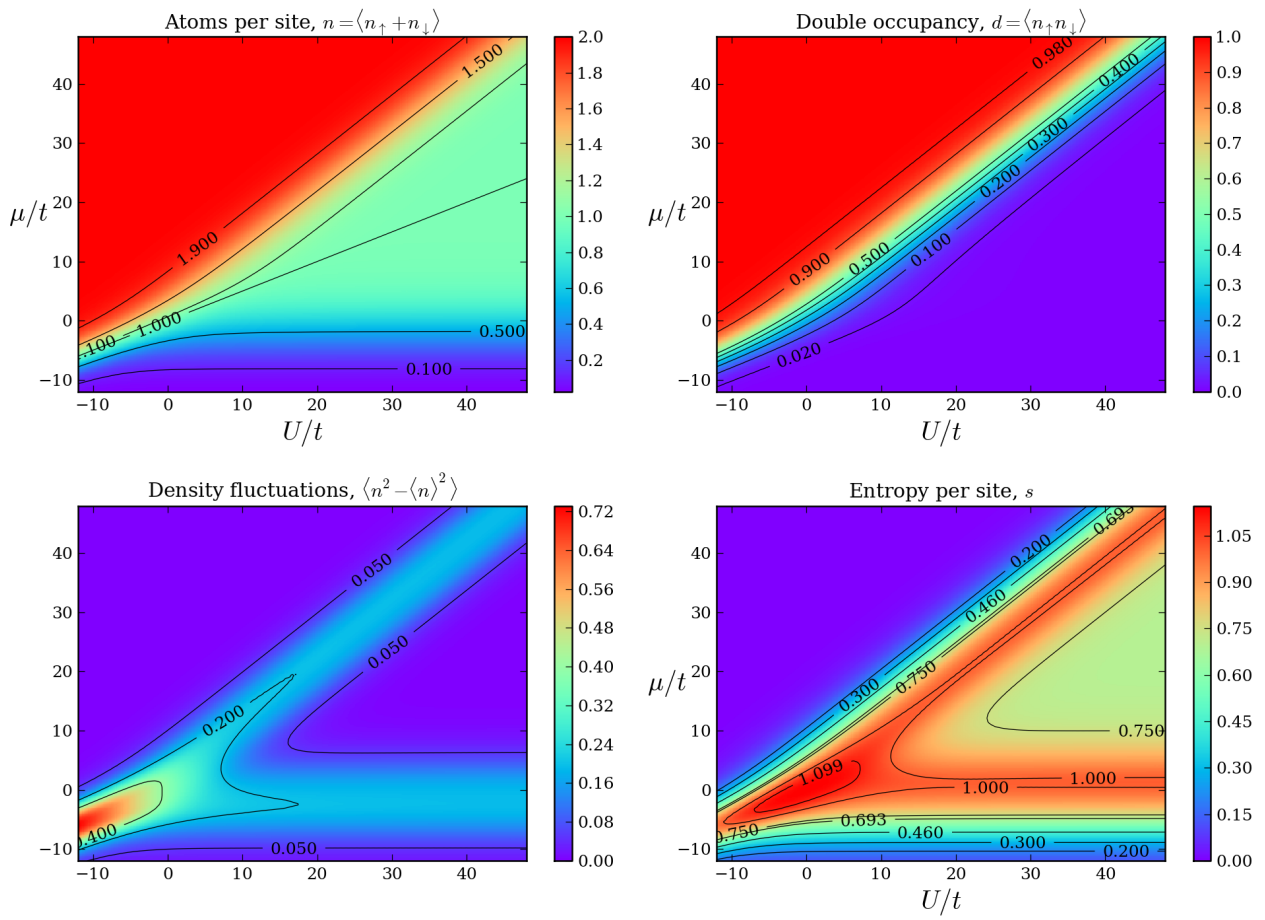

Figure 1: High temperature phase diagram of the Fermi-Hubbard model calculated using only up to the second order in the perturbation series. Temperature is given in units of tunneling, $T/t = 2.5$.

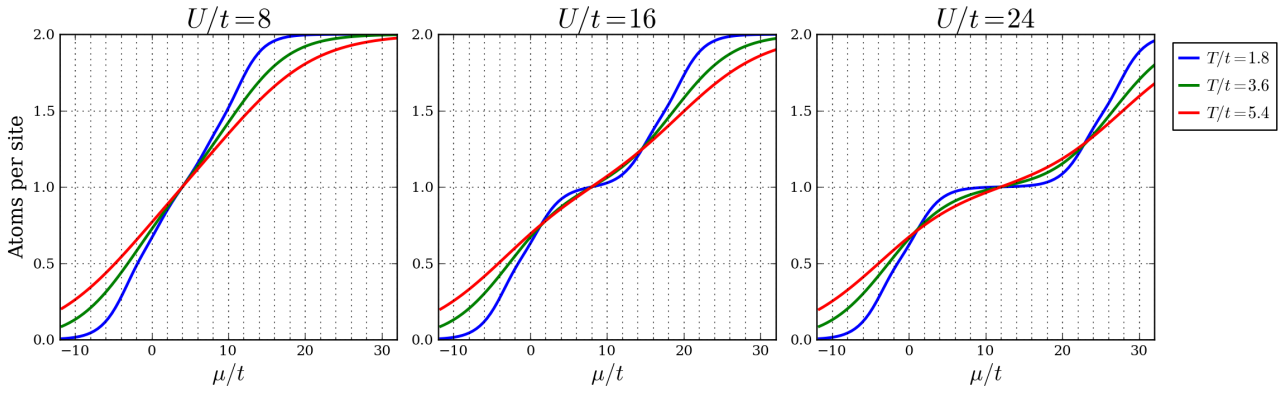

Figure 2: Density vs. chemical potential at various values of U/t and for various temperatures T/t. Calculated using only up to the second order in the perturbation series.

2 Local density approximation

In the local density approximation (LDA) we aim to establish local values for the tunneling, the on-site interactions, and the chemical potential at each point in our trap. Using these local parameters, the phase diagram for the homogeneous case can be used to calculate local thermodynamic quantities. Integrals of the local thermodynamic quantities can be directly linked to experimental observables. For example, the integral of the local density along an observation axis yields the column density, which is measured directly via in-situ phase-contrast imaging. Also, an integral over all space of the local double-occupancy yields the fraction of atoms in doubly-occupied sites. This can be measured experimentally by associating pairs of atoms into molecules (using a magnetic field sweep across a Feshbach resonance), and then measuring the number of molecules produced.

In our experiment, the lattice has an underlying confining potential and, furthermore, the lattice depth varies as a function of position in the trap. Typically, the variation of lattice depth with position in the trap is neglected when calculating the local parameters (tunneling, interactions and chemical potential) because the waists of the lattice beams are considerably large, $\gtrsim 150$ μm. In our setup, the beam waists are $\sim 45-50$ μm and we have to consider the variation of the lattice depth in the region that is sampled by the atoms.

At each point $\boldsymbol{r}$, the depth of the lattice can be different in the three orthogonal directions. The lattice depth, V_0, is then a set of three numbers $V_0(\boldsymbol{r}) \equiv \{V_{0x}(\boldsymbol{r}), V_{0y}(\boldsymbol{r}), V_{0z}(\boldsymbol{r})\}$. The hamiltonian for an atom moving in a simple cubic lattice is separable in the three spatial coordinates, so having three different lattice depths poses no problem in finding the 3D band structure, and the 3D Wannier states of the local lattice potential. On the other hand, it is more complicated to go through the calculation of the phase diagram with three different tunneling matrix elements; instead, for each $\boldsymbol{r}$, we use the average tunneling matrix element as the input for the phase diagram, in order to calculate the local thermodynamic quantities. To calculate the local on-site interactions we use integrals of the 3D Wannier states, which are simply products of 1D Wannier states for each of the three orthogonal directions.

We obtain the local chemical potential at each point in the trap as

$$\mu(\boldsymbol{r}) = \mu - E_0(\boldsymbol{r}) \tag{15}$$

The quantity $E_0(\boldsymbol{r})$ is a combination of the confining potential that envelopes the purely sinusoidal lattice potential and the zero of energy in the Fermi-Hubbard hamiltonian. In the Fermi-Hubbard hamiltonian, the kinetic energy for motion in the lattice potential is

$$-t \sum_{\langle ij \rangle, \sigma} a^\dagger_{i\sigma} a_{j\sigma} \tag{16}$$

This sum is restricted over nearest neighbors. In the microscopic derivation of the Fermi-Hubbard model there are also terms that involve a single site, but they are typically discarded because they only add a constant energy given by

$$-\sum_{i\,\sigma} t_{ii} a^\dagger_{i\sigma} a_{i\sigma} = -t_0 \sum_{i\,\sigma} n_{i\sigma} \tag{17}$$

where

$$-t_0 = \left(\frac{1}{L} \sum_{q_x} E^{1\mathrm{D}}_{q_x} + \frac{1}{L} \sum_{q_y} E^{1\mathrm{D}}_{q_y} + \frac{1}{L} \sum_{q_z} E^{1\mathrm{D}}_{q_z} \right) \tag{18}$$

It becomes clear that $-t_0$ is the average energy of the lowest band in 3D, which can be readily obtained given the set of three lattice depths along each of the orthogonal axes.

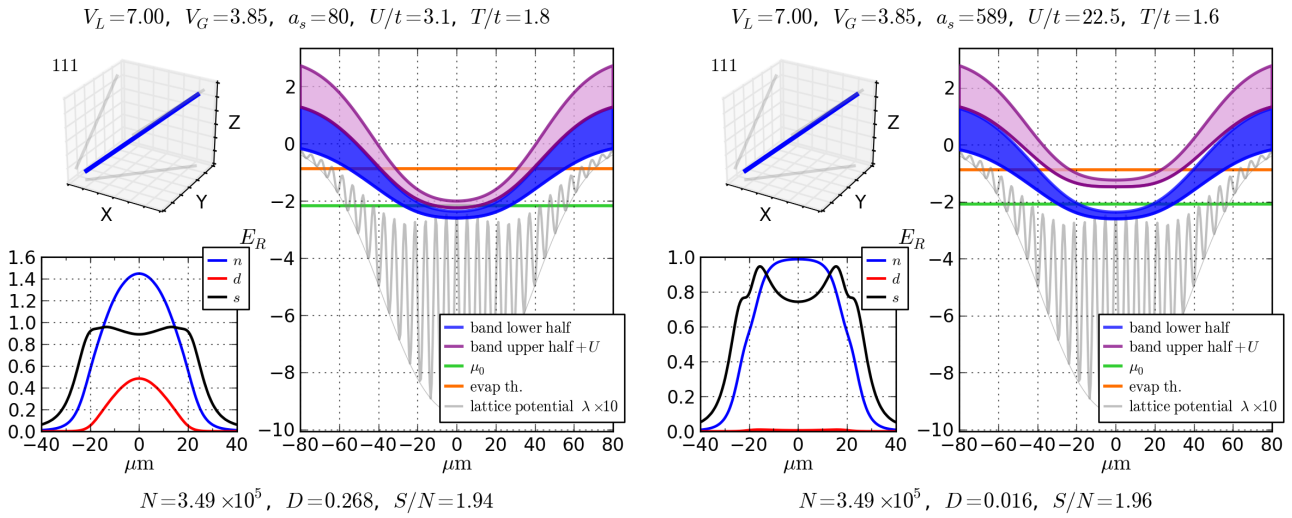

Figure 3: Illustration of the local density approximation in a compensated lattice potential. The left panel shows a situation with small interactions, obtained by setting a scattering length of 80 a_0. For the right panel the scattering length is 589 a_0. See the text for a detailed explanation.

In the most common use of the LDA in a trap, the local chemical potential is given by

$$\mu(\boldsymbol{r}) = \mu - V_{\text{trap}}(\boldsymbol{r}) \tag{19}$$

but we have seen here that to apply the local density to the lattice potential we need to consider the local band structure of the lattice, as well as the confining potential that envelopes the purely sinusoidal lattice potential. We have aggregated those two terms in the quantity $E_0(\boldsymbol{r})$. We note here that, for implementations with large lattice beam waists, the lattice depth can be taken as a constant over the region occupied by the atoms. This means that the local band structure does not vary over the sample, and the quantity $E_0(\boldsymbol{r})$ can be replaced by only the confining potential. This is the typical way in which LDA is applied to a lattice [4, 5, 6, 7], except for the treatment in [8] which takes into account the length scales set by the waists of the lattice beams.

We show in Fig. 3 an illustration of the application of the LDA to a compensated lattice potential. On the left the scattering length is 80 a_0, which corresponds to a relatively small $U/t = 3.1$ at the center of the lattice. On the right, the scattering length is 589 a_0, which corresponds to $U/t = 22.5$ at the center. All of the lines plots are along the 111 direction, as illustrated on the top left inset in each panel.

The larger plot on the right of each panel shows the 3D band structure, the global chemical potential, the lattice potential, and the threshold for evaporation. The sinusoidal lattice potential is enveloped at the bottom by an overall confinement that results from the lattice beams plus the contribution from the green compensation beams. The lattice modulation is shown, with the wavelength scaled ×10 for clarity. The depth of the modulation corresponds to the smallest of the three lattice depths $V_{0x}(\boldsymbol{r})$, $V_{0y}(\boldsymbol{r})$, $V_{0z}(\boldsymbol{r})$ at a given point, $\boldsymbol{r}$, in the trap. Along the 111 direction we have $V_{0x} = V_{0y} = V_{0z}$.

The 3D band structure is shown with the shaded blue and purple areas. The blue area shows the lower half of the band. The bottom of the blue area corresponds to the lowest available single particle energy level. The top of the blue area corresponds to the average energy of the lowest band, which is exactly the quantity $E_0(\boldsymbol{r})$ that we defined above. The local chemical potential is measured with respect to $E_0(\boldsymbol{r})$. The purple area shows the upper half of the band plus the contribution from the on-site interactions. The spacing between $E_0(\boldsymbol{r})$ and the bottom of the purple band corresponds to the Mott gap at zero temperature.

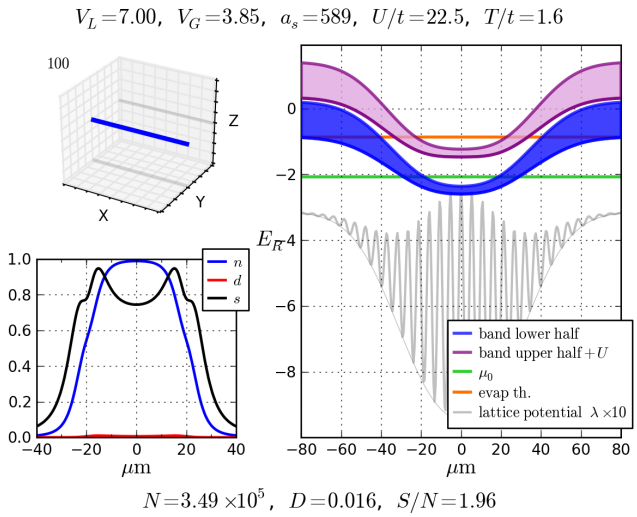

Figure 4: Illustration of the local density approximation in a compensated lattice potential. Line plot along 100 for a scattering length of 589 a_0. See the text for a detailed explanation.

On the bottom left of each panel in Fig. 3 we show the local thermodynamic quantities, namely the number of particles per site (n), the double-occupancy per site (d), and the entropy per site (s). On the left, at 80 a_0, we see that the interactions are not strong enough to have a Mott insulating state, and the density at the center is above one particle per site. On the right, at 589 a_0 the density is capped at one per site at the center of the trap due to the large value of the on-site interactions.

The orange line, which is labeled as the evaporation threshold, is better understood if we make a line plot along one of the lattice directions, for instance 100. This is shown in Fig. 4. The evaporation threshold is the energy that a particle needs to escape along one lattice beam. If it has enough energy, the particle can escape the central part of the trap by tunneling along a lattice direction. The situation is slightly different than in a non-lattice potential, since the velocity of escape will be reduced due to the presence of the lattice, and furthermore the particle may Bragg scatter off of the lattice and be kicked back towards the center of the trap.

2.1 Validity of the local density approximation

The LDA breaks down at low temperatures, where long range correlations become important for the description of the system. In the high temperature series expansion, the correct solution at lower temperatures can only be obtained if sufficient orders in the series are considered. We recall that the n^{th} term in the series can be associated to a particle tunneling n times and returning to its original position. That means that the particle must explore a region of size $a\sqrt{n}$, where a is the lattice spacing. If the values of the local parameters (t, U, and μ) vary considerably over $a\sqrt{n}$, then the applicability of the local density approximation for the series solution stops making sense. This will inevitably happen at low enough temperatures, where long range correlations start to develop in the system. The break-down of LDA makes it very challenging to consider inhomogeneous systems at low temperatures. At the same time, the most interesting physics is associated with the appearance of long range order and the resulting phase transitions that occur at low enough temperatures. The prime example is the transition from a Mott insulator to an antiferromagnetic Mott insulator, which is expected to happen at a temperature of around $T/t \sim 0.3 - 0.4$ [9, 10, 7, 11].

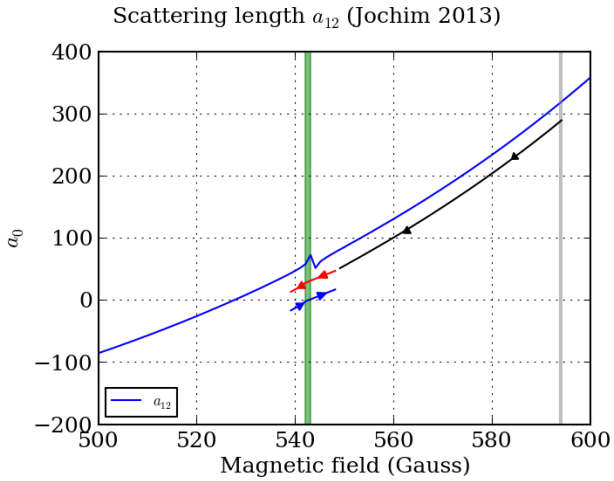

Figure 5: Scattering length as a function of magnetic field in the region relevant for simulation of the repulsive Fermi-Hubbard model. The scattering length data is obtained from [12]. The vertical green line marks the position of the narrow Feshbach resonance. The arrows show the magnetic field sweeps that are used to go from the initial value of the scattering length to a value approaching the narrow resonance (black), then sweep across the resonance to associate doubly-occupied sites into molecules (red), and then back across the resonance do dissociate the molecules back into atom pairs (blue).

3 Experimental measurement of the double-occupancy and comparison with the LDA

In our experiment we can measure double-occupancies by making use of the narrow Feshbach resonance at 543 G. The scattering length as a function of magnetic field is shown in Fig. 5. We perform our lattice loading ramps as usual, reaching a lattice depth of $7\,E_R$ with a green compensating potential of $4\,E_R$. The scattering length is set to the desired value during the lattice loading ramps. After the final parameters are reached, the lattice depth is suddenly increased to $50\,E_R$ (at the center of the trap) in order to prevent any further motion of particles. After this is done, we first ramp the magnetic field in 8 ms down to 80 a_0; from there we go across the resonance to 61 a_0 in 24 ms. Pairs of atoms in doubly occupied sites are associated to create molecules when the magnetic field is ramped across the resonance. The resulting molecules are far detuned with respect to the free atoms, so we can take an in-situ phase contrast image to reveal the distribution of atoms in singly occupied sites.

At this point we can also opt to blow away the atoms using a resonant light pulse, and then sweep the magnetic field back across the resonance to dissociate the molecules. In this way we can directly image the in-situ distribution of doubly-occupied sites. At the moment we do not have the data for the direct double-occupancy measurement. We were technically limited by our inability to blow away single atoms in both of the spin states in a time small compared to the lifetime of the molecules. Even though we are at $50\,E_R$ we observe a finite lifetime of the molecules which depends on the number of atoms in singly occupied sites. We believe, as was suggested in [13], that the fast molecular decay is due to atoms that tunnel to a site that has a molecule and inelastically collide with it.

The data that we have at the moment consists of pictures of the in-situ density distribution taken at three different times in the sequence:

1. Right before locking the lattice to $50\,E_R$. Lattice depth is $7\,E_R$.
2. Right after locking the lattice to $50\,E_R$.

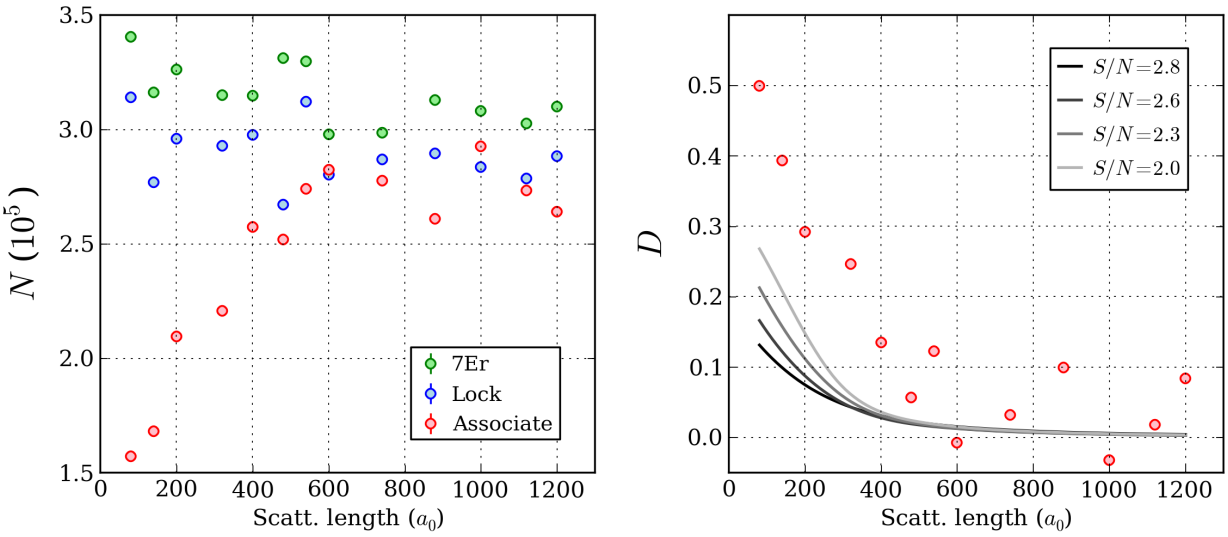

Figure 6: Measurement of the fraction of atoms in doubly occupied sites as a function of scattering length. The left panel shows the atom number measured in-situ (green points) in a $(7.5, 7.5, 8.5)\, E_R$ lattice (Note: We were aiming for a $7\, E_R$ lattice but we had a bad calibration of the lattice depths, see Section 4.2), at $50\, E_R$ after locking the lattice (blue points), and after associating atoms in doubly occupied sites to form molecules (red). The right panel shows the fraction of atoms in doubly occupied sites and the results obtained from the LDA at various values of total entropy per particle. (In this figure each point is from a single experimental run. We plan to take more data so that we can do a better average at each point and include an error bar.)

3. Right after performing the magnetic field sweep that associates doubly-occupied site into molecules.

With this data, we integrate the in-situ density distributions to obtain the total fraction of atoms in singly occupied sites. The complement of this is the total fraction of atoms in doubly occupied sites, D. The image of the atoms in singly occupied sites is taken only a few milliseconds after crossing the Feshbach resonance. This should minimize systematic effects, due to atom losses from inelastic collisions with molecules. In any case, the measurement should be strictly considered as a lower bound on the number of atoms in singly occupied sites. The complement, D, is then an upper bound on the total fraction of atoms in doubly-occupied sites.

Using the LDA, as shown in Section 2, we can obtain local values of the thermodynamic quantities at any position in our trap. We integrate the local double-occupancy to find D, which can then be compared to the experimentally determined quantity. The results are shown in Fig. 6.

We see that the fraction of atoms in doubly-occupied sites that we observe is larger than what is expected from the LDA and the high temperature series expansion to second order. In the LDA, for a given U/t, D increases for lower entropy. This is contrary to intuition, as one expects double occupancies to be thermally activated in the system. In the trapped system, the increase in D with entropy is a consequence of the reduction of the central density at higher entropy. This point is made in [14], where a detailed study of the double-occupancy as a function of characteristic filling[2] and interaction strength was performed with ^{40}K atoms in a simple cubic lattice.

It is also pointed out in [6] that, even for the homogeneous model, the double-occupancy can be enhanced in the antiferromagnetic core since each atom is surrounded by only opposite spins. An atom can lower its energy in a second order process by virtually hopping to any of the nearest neighbors. In contrast,

[2]Characteristic filling is $\rho = N/N_0$ where N_0 is the number of atoms per spin that produces half filling in the center of the trap at zero temperature and without interactions [14].

in the paramagnetic state, half of the neighbors are of the same spin, so tunneling to those sites is forbidden by the Pauli principle. It is shown in [6] that such an enhancement is significant only for $U/t > 9$, so it cannot be really related to the large value of D that we observe for the smaller values of U/t.

An interesting result shown in [6] is related to the column integral of the local double occupancies. It is shown there that the double-occupancy profile somewhat resembles the shape of the antiferromagnetic core, and thus could be used as an indicator of its presence.

Other experiments typically perform double-occupancy measurements in time-of-flight, however we have the possibility of accessing the in-situ double-occupancy using phase-contrast imaging. An in-situ measurement of the double-occupancy would involve associating atom pairs, then blowing away free atoms with a resonant pulse, then dissociating the remaining molecules and imaging them using in-situ phase-contrast imaging. A technical limitation forced us to wait about 70 ms in between blow away pulses for atoms in states $|1\rangle$ and $|2\rangle$. This wait is too long given the short lifetime of the molecules in the lattice. We have since overcome the time limitation and we can blow away the two states simultaneously (but we have not taken the data yet). This should allow us to circumvent the short lifetime of the molecules and take in-situ data for the double-occupancy.

Furthermore the direct measurement of the double-occupancy would allow us to put a lower bound on D, which would address the possibility that the larger D that we observe is due to a systematic overestimation.

4 Latest Bragg scattering data as a function of scattering length

Lately we have been trying to get final data on the Bragg scattering signal as a function of the scattering length. Our main issue continues to be the stability and reproducibility in aligning the compensated lattice potential.

The data that we have taken so far is shown in Fig. 7. We do our usual lattice loading ramps, then we suddenly ramp up the lattice to $20\,E_R$ and probe with the Bragg beam. We tried using a $50\,E_R$ lattice lock, but the Bragg signal was not as strong we suspect that it has to do with the speed of the lock ramps. Doing any further studies on that variable is expensive in time, so we decided to stick to the $20\,E_R$ ramp which happens in about $150\,\mu$s (limited by our intensity stabilization circuitry). The main point that stands out is that we observe the largest AFM correlations in a U/t region where the fraction of atoms in doubly occupied sites is still considerably large. We are extending this question to our theory collaborators in hope of a better understanding of what is going on.

Below we enumerate a few points:

1. The best indicator of AFM correlations should be in $A2_t$.
    - However, this measure is also susceptible to any suppression of light scattering due to the presence of double occupancies. This may have something to do with the < 1 point at 80 a_0 for $A2_t$. For more information on the suppression of light scattering due to double occupancies see Sec. 4.1.
    - A technical problem with $A2_t$ is that in-situ shots and TOF shots come from different experimental runs. So this measure has added noise due to atom number variations and probe intensity variations from shot to shot .
2. There is suppression of light scattering in $A1_t$.

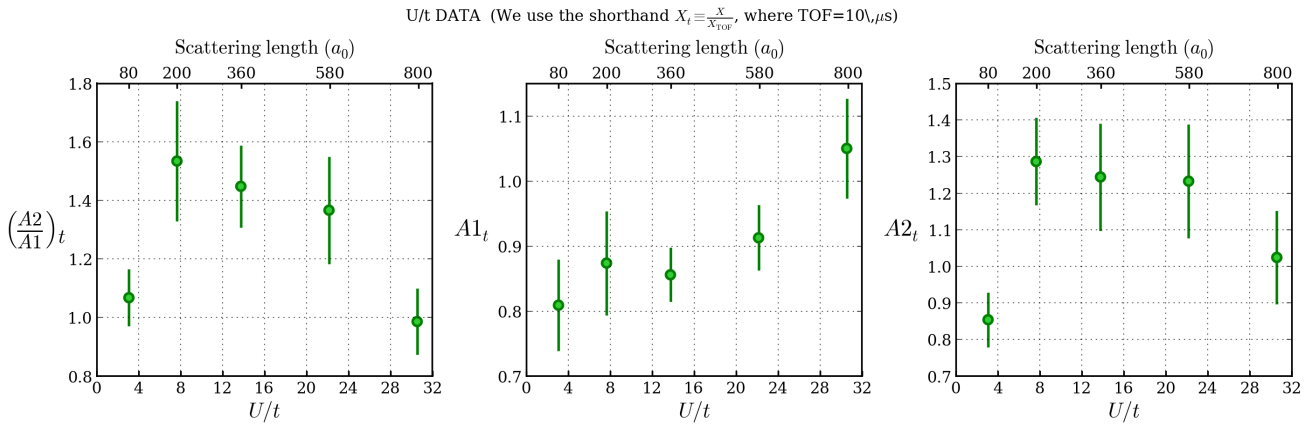

Figure 7: $\left(\frac{1}{2}\ \frac{1}{2}\ \frac{1}{2}\right)$ Bragg scattering as a function of scattering length.

- One may suggest that this comes from a strong AFM Bragg scattering signal that we may be missing due to bad placing of the input Bragg beam or the $A2$ camera. We have attempted to vary the input Bragg beam angle and the $A2$ camera angle to try to find a steep slope on $A2_t$ but we have found nothing. This makes us believe that the angular distribution of Bragg scattering is broad (as we learned from our previous rocking curve data) and that the suppression observed here in $A1_t$ is related to the double occupancies at the lower scattering lengths.

3. The signals that we obtain are noisy because we do not have many photons reaching our cameras.
   - A nice feature of $A2/A1$ is that noise due to shot-to-shot atom number and probe variations is canceled out because $A2$ and $A1$ can be recorded simultaneously for every shot.

4.1 Suppression of light scattering due to the presence of double-occupancies

A few weeks ago we studied briefly the suppression of light scattering due to the presence of double-occupancies. To do this, we created sample with only doubly-occupied sites. This was done by sweeping through the Feshbach resonance, blowing away singly occupied sites and then dissociating the resulting molecules. At a lattice depth of $50\,E_R$, we observed a suppression in the scattered light in the in-situ pictures for a probe light detuning in between the two hyperfine states. This is shown in Fig. **??**. For reference we show the Debye-Waller factors for the several directions, including $\boldsymbol{k}_{in}$ =#1, #5, in Fig. 9

4.2 Disclaimer and what's next

In between taking the doublon data and the Bragg data we had to recalibrate the lattice beams. This resulted in a correction so that the doublon data is not at $7\,E_R$ lattice depth as we intended, but more likely at lattice depths of $7.5, 7.5, 8.5,\ E_R$ in each of the three directions. Our aim right now is to take more Bragg data in order to reduce the size of the error bars in the U/t curve. After we are done with this, we want to follow up with the doublon data and using the capability of measuring the double-occupancy in-situ.

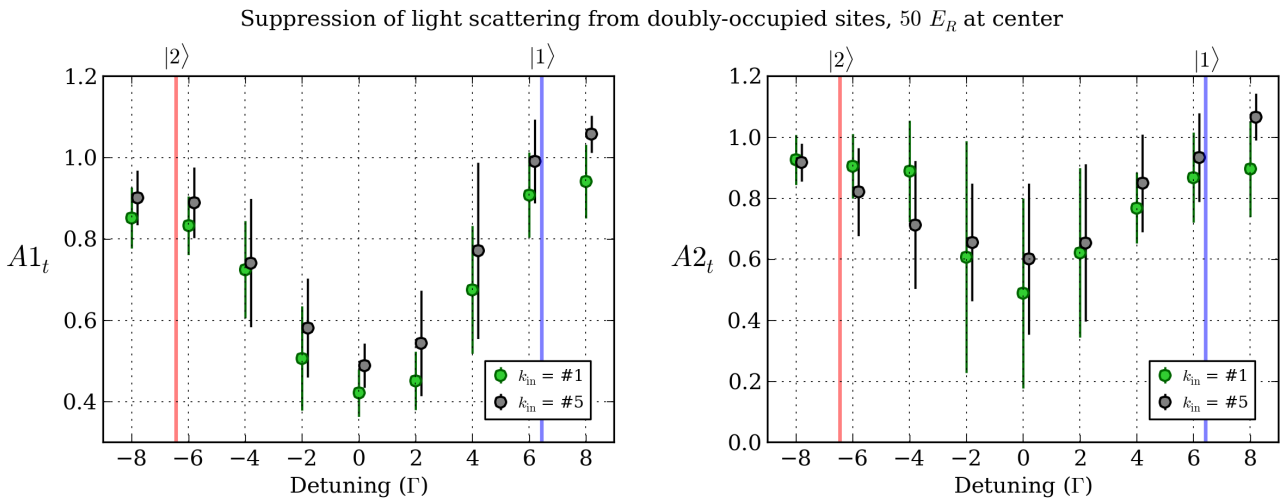

Figure 8: Suppression of light scattering from doubly-occupied sites. The suppression is strongest for a detuning in between the two hyperfine states. This is the same detuning used in the spin sensitive $\left(\frac{1}{2}\ \frac{1}{2}\ \frac{1}{2}\right)$ Bragg scattering.

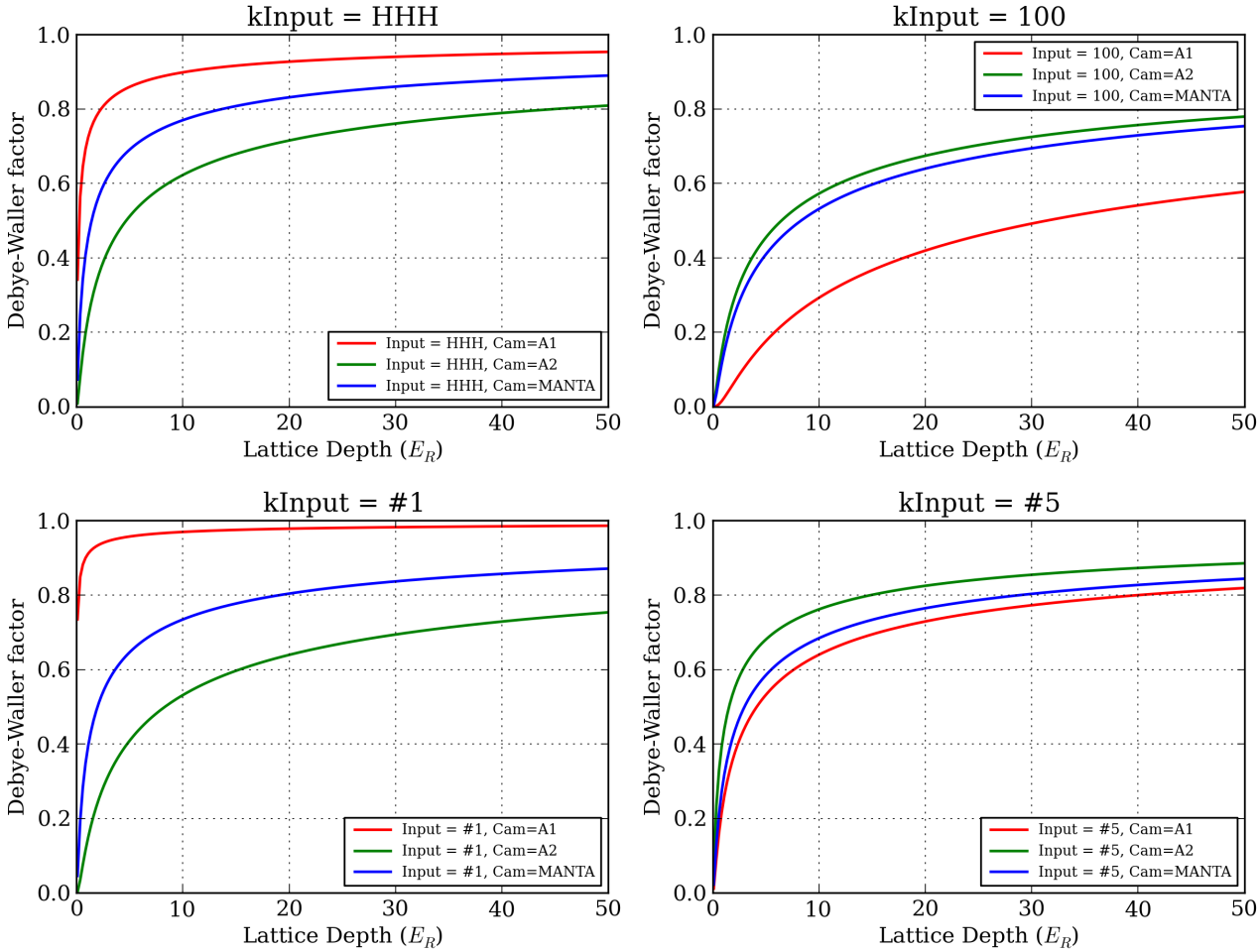

Figure 9: Debye-Waller factor for various inputs as a function of lattice depth.

References

[1] J. Henderson, J. Oitmaa, and M. Ashley, "High-temperature expansion for the single-band Hubbard model," Physical Review B **46,** 6328–6337 (1992).

[2] R. Jördens, Ph.D. thesis, ETH Zürich, 2010.

[3] R. Scalettar, "QUEST: QUantum Electron Simulation Toolbox,", `http://quest.ucdavis.edu/tutorial/hubbard7.pdf`, 2013.

[4] L. De Leo, C. Kollath, A. Georges, M. Ferrero, and O. Parcollet, "Trapping and Cooling Fermionic Atoms into Mott and Néel States," Physical Review Letters **101,** 210403 (2008).

[5] L. De Leo, J.-S. Bernier, C. Kollath, A. Georges, and V. W. Scarola, "Thermodynamics of the three-dimensional Hubbard model: Implications for cooling cold atomic gases in optical lattices," Physical Review A **83,** 023606 (2011).

[6] E. V. Gorelik, I. Titvinidze, W. Hofstetter, M. Snoek, and N. Blümer, "Néel Transition of Lattice Fermions in a Harmonic Trap: A Real-Space Dynamic Mean-Field Study," Physical Review Letters **105,** 065301 (2010).

[7] S. Fuchs, E. Gull, L. Pollet, E. Burovski, E. Kozik, T. Pruschke, and M. Troyer, "Thermodynamics of the 3D Hubbard Model on Approaching the Néel Transition," Physical Review Letters **106,** 030401 (2011).

[8] C. J. M. Mathy, D. a. Huse, and R. G. Hulet, "Enlarging and cooling the Néel state in an optical lattice," Physical Review A **86,** 023606 (2012).

[9] R. Staudt, M. Dzierzawa, and A. Muramatsu, "Phase diagram of the three-dimensional Hubbard model at half filling," The European Physical Journal B **17,** 411–415 (2000).

[10] P. Kent, M. Jarrell, T. Maier, and T. Pruschke, "Efficient calculation of the antiferromagnetic phase diagram of the three-dimensional Hubbard model," Physical Review B **72,** 060411 (2005).

[11] T. Paiva, Y. L. Loh, M. Randeria, R. T. Scalettar, and N. Trivedi, "Fermions in 3D Optical Lattices: Cooling Protocol to Obtain Antiferromagnetism," Physical Review Letters **107,** 086401 (2011).

[12] G. Zürn, T. Lompe, a. N. Wenz, S. Jochim, P. S. Julienne, and J. M. Hutson, "Precise Characterization of ĝ6Li Feshbach Resonances Using Trap-Sideband-Resolved RF Spectroscopy of Weakly Bound Molecules," Physical Review Letters **110,** 135301 (2013).

[13] G. Thalhammer, K. Winkler, F. Lang, S. Schmid, R. Grimm, and J. H. Denschlag, "Long-Lived Feshbach Molecules in a Three-Dimensional Optical Lattice," Physical Review Letters **96,** 050402 (2006).

[14] R. Jördens *et al.*, "Quantitative Determination of Temperature in the Approach to Magnetic Order of Ultracold Fermions in an Optical Lattice," Physical Review Letters **104,** 180401 (2010).